



HAL
open science

Ex-situ catalytic upgrading of pyrolysis vapors using mixed metal oxides

W. Locatel, D. Laurenti, Y. Schuurman, N. Guilhaume

► **To cite this version:**

W. Locatel, D. Laurenti, Y. Schuurman, N. Guilhaume. Ex-situ catalytic upgrading of pyrolysis vapors using mixed metal oxides. *Journal of Analytical and Applied Pyrolysis*, 2021, 158, 10.1016/j.jaap.2021.105241 . hal-03335161

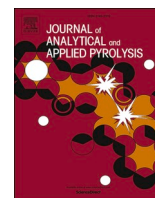
HAL Id: hal-03335161

<https://hal.science/hal-03335161>

Submitted on 15 Nov 2021

HAL is a multi-disciplinary open access archive for the deposit and dissemination of scientific research documents, whether they are published or not. The documents may come from teaching and research institutions in France or abroad, or from public or private research centers.

L'archive ouverte pluridisciplinaire **HAL**, est destinée au dépôt et à la diffusion de documents scientifiques de niveau recherche, publiés ou non, émanant des établissements d'enseignement et de recherche français ou étrangers, des laboratoires publics ou privés.



Ex-situ catalytic upgrading of pyrolysis vapors using mixed metal oxides

William de Rezende Locatel, Dorothee Laurenti, Yves Schuurman, Nolven Guilhaume *

Univ. Lyon, CNRS, IRCELYON – UMR 5256, 2 Avenue Albert Einstein, Villeurbanne Cedex, F-69626, France

ARTICLE INFO

Keywords:

Biomass pyrolysis
Bio-oils
Catalytic upgrading
Nb-based oxides
Brønsted/Lewis acidity

ABSTRACT

Ex-situ catalytic fast pyrolysis (CFP) was employed to produce bio-oils from beech wood. The effect of Nb-based mixed oxides (with second metal oxide = W, Al or Mn) in upgrading the pyrolysis vapors was compared to an H-ZSM-5 catalyst and to non-catalyzed pyrolysis. The catalysts acidic properties were assessed by NH_3 -TPD and FTIR of adsorbed pyridine. The bio-oils obtained were characterized by Karl-Fischer titration, GPC, CHNS analyses, ^{13}C -NMR, GC-MS, GCxGC-MS. In spite their very different acidic properties, the $\text{Nb}_x\text{Mn}_y\text{O}_z$ catalyst (with essentially Lewis acid sites) exhibited similar performances as H-ZSM-5 (that presents a high density of Brønsted sites), in terms of liquid phase selectivity and reduction of oxygen content in the bio-oils produced. These observations were accompanied by a reduction of compounds such as acids, aldehydes, ketones, ethers and sugars that contribute to the detrimental properties of bio-oils. Finally, the results suggest that the Lewis acid sites of $\text{Nb}_x\text{Mn}_y\text{O}_z$ are converted into Brønsted sites in the presence of water vapor produced by pyrolysis of wood, whereas the strongest Brønsted sites of H-ZSM-5 have a limited impact on the upgrading process due to their limited accessibility for most components of pyrolysis vapors.

1. Introduction

In order to reduce the fossil fuels dependency, the European Parliament and Council implemented the Renewable Energy Directive (RED) in 2009 (Directive 2009/28/EC). One objective of this energy policy was to increase the percentage of renewable fuels in the European energy matrix. On its last revision in 2018, it was stipulated the target of at least 32 % of renewable energy in 2030 [1]. An alternative to reduce fossil fuels dependency without heavy investment on new refineries is to increase the percentage of renewable energy in co-processing bio-oils derived from lignocellulosic biomass with conventional fossil feedstocks. An advantage of this strategy is the possibility to use the existing refinery structures, reducing investment costs [2]. However, the integration of bio-oil in this process faces some technical difficulties such as their high oxygen content, poor miscibility with hydrocarbon fuels, low chemical stability, high acidity, low heating value, high moisture content [3]. Therefore, it is necessary to improve bio-oils quality before mixing them with traditional oils to produce fuels. One possible option is to reduce the oxygen content through hydrodeoxygenation (HDO), however, this upgrading step requires high hydrogen pressures (up to 200 bar [4]) and consumption [5]. An alternative option is *ex-situ* catalytic fast pyrolysis (CFP), in which the vapors produced by thermal pyrolysis are converted on a catalyst before their condensation, at

atmospheric pressure [6]. In the first step, the fast pyrolysis of lignocellulosic biomass is realized at high temperature range (400–600 °C) [7] with short residence time (~1 s) [8]. Then, in a second step, the vapors are driven on the catalytic bed where the upgrading reactions occur. As a result, the condensed oil has a superior quality due to the conversion of unstable and reactive compounds and to the reduction of the overall oxygen content.

With this reactor configuration, the catalyst and biomass are not in direct contact, which prevents the catalyst deactivation by ash deposition or its contamination and gives the possibility of using optimal conditions for each process (pyrolysis of biomass and vapor reforming) [9,10].

Zeolite-based catalysts, especially H-ZSM-5, are the most studied catalysts to improve the quality of bio-oils due to their high activity and selectivity for hydrocarbons production and the capability to reduce the formation of undesirable products, such as carboxylic acids and oxygenated compounds [11]. However, zeolites are susceptible to deactivation, essentially through coking [12], which affects operational costs of the process and reduces its competitiveness compared with fuel production from exclusively fossil feedstocks [8,13]. As an alternative for traditional catalysts, metal oxides can display acidic properties and good resistance to coke formation [14]. Among them, niobium-based oxides has been studied in heterogeneous catalysis [15], but have not

* Corresponding author.

E-mail address: nolven.guilhaume@ircelyon.univ-lyon1.fr (N. Guilhaume).

<https://doi.org/10.1016/j.jaap.2021.105241>

Received 11 March 2021; Received in revised form 21 June 2021; Accepted 22 June 2021

Available online 3 July 2021

0165-2370/© 2021 The Authors.

Published by Elsevier B.V. This is an open access article under the CC BY-NC-ND license

(<http://creativecommons.org/licenses/by-nc-nd/4.0/>).

been assessed in upgrading of pyrolysis vapors. Niobium oxide exhibits both Brønsted and Lewis acidity, and its acidic properties can be promoted by introduction of other acidic oxides such as W, Al and Mn oxides.

The aim of this work was to synthesize, characterize and evaluate different niobium-based metal mixed oxides in the ex-situ conversion of wood pyrolysis vapors. These mixed metal oxides with different acidities were compared to a H-ZSM-5 catalyst.

2. Materials and methods

2.1. Biomass

The feedstock consists of beech wood chips with particle size in the range 0.75–2.5 mm, supplied by J. Rettenmaier & Söhne (JRS). Its bulk density was measured by weighing the amount of sample contained in a volume of 100 mL. The ash content was obtained by calcining wood samples at 600 °C for 3 h (1 °C/min) under air. The moisture content was determined by weight difference between the raw sample and the sample dried at 110 °C for 1.5 h, keeping the dry sample in a desiccator while cooling down to room temperature before weighing in an hermetically sealed flask. For the determination of extractives, the biomass was dried at 110 °C for 1 h. 6 g of beech wood chips were extracted with n-hexane using an automatic solvent extractor (SER 158 – Velp Scientifica) for 4 h. Then, the process was repeated over the same sample using acetone as solvent. This methodology was adapted from the work of Zule and Moze [16].

The thermal degradation of the wood was studied by thermal gravimetric analysis (TGA), under air or N₂ at temperatures between 25 °C and 900 °C (10 °C/min) on a Setsys Evolution 1200 (SETARAM) thermogravimetric analyzer. Elemental analysis (CHNS) was carried out in an equipment Flash2000 (Thermo Scientific). Scanning Electron Microscopy (SEM) was performed using a JEOL JSM 5800 L V microscope equipped with an EDS analyzer.

2.2. Catalyst preparation

The chemicals were purchased from Sigma-Aldrich or Merck and used without further purification. The catalysts were prepared by the citrate gel method. Initially, the precursor salts of metal oxides (ammonium niobate^V oxalate hydrate, ammonium metatungstate hydrate, aluminum nitrate nonahydrate or manganese (II) nitrate hydrate) and citric acid were mixed in demineralized water in an appropriate proportion aiming to obtain the following molar ratios: citric acid/(Nb + M) = 2, Nb/M = 1.5. The pH was adjusted to 7 using ammonia aqueous solution (32 %) and the solution was heated at 90 °C under stirring to evaporate the water until a viscous gel was obtained (about 2 h). This gel was dried in an oven at 170 °C for 12 h and the resulting powder was crushed then calcined at 600 °C for 3 h (1 °C/min) under a flow of air. Finally, the catalyst powder was sieved to a particle size between 100 and 300 μm. The catalysts obtained were named as Nb_xM_yO_z where M = W, Al or Mn. In addition, a pure niobium oxide catalyst was prepared using the same procedure.

The H-ZSM-5 catalyst sample with a Si/Al ratio of 40 was supplied by Céramiques Techniques Industrielles (CTI) Salindres, France. It was calcined and sieved similarly to the Nb-based catalysts.

2.3. Catalyst characterization

The metal contents were obtained by chemical analysis using inductively coupled plasma optical emission spectrometry (ICP-OES) performed on an Activa (Jobin Yvon).

The presence of crystallized phases and their identification were obtained using a Bruker D8 Advanced A25 diffractometer, equipped with radiation Cu Kα₁₊₂ (λ = 1.5 Å) and detector LynxEye, with 2θ from 4° to 80° and step of 0.02°.

The textural properties of catalysts were characterized by nitrogen adsorption at –196 °C on a Belsorp II adsorption measurements apparatus. Before the analysis, the samples (about 300 mg) were desorbed at 200 °C under vacuum overnight. The specific surface area and total pore volume were estimated using the Brunauer-Emmett-Teller (BET) equation and the Barrett-Joyner-Teller (BJH) method was applied to calculate the average pore diameter.

The total acidity of catalysts was quantified by NH₃-TPD using a Belcat M apparatus equipped with a thermal conductivity detector. The samples were pretreated at 600 °C prior to NH₃ adsorption at 100 °C, followed by TPD under He. The Brønsted/Lewis acidic properties of the solids were assessed by Fourier Transform Infrared spectroscopy (FT-IR) using pyridine as probe molecule. This analysis was carried out using self-supported wafer of catalyst with 14 mm of diameter. Prior to pyridine adsorption, the samples were treated at 450 °C overnight under vacuum. Then, the background IR spectrum was recorded. Afterward, adsorption of pyridine was performed at room temperature for 15 min and then, pyridine desorption was performed under vacuum at 150, 250, 350 and 450 °C for 1 h. IR spectra were recorded at room temperature on a Nicolet Magna-550 spectrometer. The spectra of pyridine adsorbed on the catalysts were obtained by subtraction of the background spectrum.

2.4. Pyrolysis set-up

A pyrolytic set-up already described previously [17] was used after some modifications. The wood chips were dried at 110 °C for 1.5 h before being placed in a gas-tight hopper and kept under N₂. A solid dispenser allowed a semi-continuous delivery of the wood chips (every 2.5 s), with a feeding rate of 20 g/h. The wood chips fall by gravity in a quartz tubular reactor equipped with internal spikes to slow down the fall and increase the residence time of wood particles in the pyrolysis

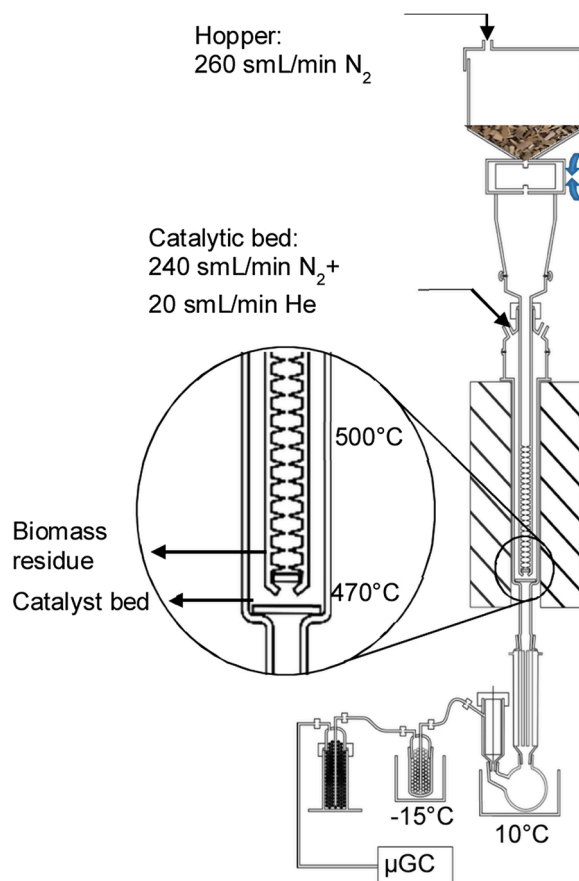


Fig. 1. Scheme of pyrolysis set-up.

section (Fig. 1). In the reactor, a first quartz frit stops the solid residues, while the vapors are driven through the catalytic bed placed downstream on a second frit.

The reactor was heated by a tubular oven which regulated the pyrolysis section temperature to 500 °C and the catalyst temperature to 470 °C. Two inert gas flows were dispensed separately in the two reactor parts: 260 s ml/min of N₂ from the wood hopper to the pyrolysis section of the reactor (this flow serves to keep the wood chips under inert atmosphere and to drive the pyrolysis vapors towards the catalyst bed) and 240 s ml/min of N₂ + 20 s ml/min of He (internal standard) sent directly to the catalytic bed (this flow is used to prevent retro-diffusion of vapors and to adjust the total gas flow rate). A trap system including A) a condenser and a round bottom flask at 10 °C, B) an electrostatic precipitator, C) a trap filled with Pyrex beads at -15 °C and D) a silica gel beads trap at ambient temperature, prevents any condensable liquids from reaching the on-line micro-GC analyzer. The main part of the bio-oils was directly recovered in the first cold trap at 10 °C, but other portions were also recovered downstream in the different parts of the glassware assembly (cold traps, electrostatic precipitator, Pyrex and silica gel beads). The total mass of bio-oils formed in the experiments was established by mass difference, by weighing the different glassware parts before and after the experiments. The mass of solid residue deposited on the first frit glass was weighed, whereas the gaseous products were quantified by GC and converted to a mass of gaseous products, in order to determine the mass balance of gas, liquid and solid products. In catalytic experiments, 2 g of catalyst were used (discounting the water content determined by TGA) and before starting the wood delivery, the reactor was heated to 500 °C for 1 h in order to reach a stable temperature and to desorb the catalysts.

2.5. Products analysis

2.5.1. Gas phase composition

The non-condensable products were analyzed on-line using a micro gas chromatograph Inficon 3000 (SRA instruments) equipped with three analytical modules (MolSieve, Plot U and Alumina columns) in order to identify and quantify all the gaseous compounds produced (He, H₂, CO, CO₂ and C₁-C₅ hydrocarbons). Each analysis duration was 6 min and they were run successively for 90 min. The GC response of all gaseous compounds was calibrated using appropriate calibration mixtures. Helium was used as internal standard for quantitative analysis, because the production of gaseous compounds resulted in a net effluent flow rate higher than the inlet flow rate.

2.5.2. Bio-oil analysis

The water content of bio-oils was determined by Karl-Fischer Titration, using a Titrand 852 from Metrohm. The samples were diluted in methanol (≈ 2 %wt. of oil) and the colorimetric method was employed.

The average molar mass and molar mass distribution of organic fraction readily recovered was obtained by gel permeation chromatography (GPC). The measurements were performed with an Agilent equipment (1200 series) using two PL gel columns with different pore size (500 and 50 Å) equipped with a refractive index detector (RID) and a UV detector operating at 254 nm. The mobile phase used was THF with flowrate of 1 mL/min. Bio-oil samples were diluted in THF with a concentration of 1 wt% and filtered (0.45 μm) before analysis. These analyses were performed at 35 °C and the system was calibrated using hydrocarbons (HC) standards with molecular weights between 86 and 1000 g/mol. This calibration was preferred over calibration with polystyrene (PS) standards because the MW of two reference compounds that can be considered as lignin model compounds, eugenol (164 g/mol) and 1-(2,4-Dihydroxyphenyl)-2-(4-methoxyphenoxy)ethenone (DHPMPE, 274 g/mol) were determined more accurately when the HC calibration was applied (-4% and -15 %, respectively with HC calibration, whereas PS calibration led to strongly overestimated MW (+57 % and +70 %, respectively).

The ¹³C-NMR spectra were recorded with a spectrometer Bruker AVANCE 400 MHz and the spectra were analyzed using TopSpin 3.0 software. Each sample was analyzed with 6000 scans at room temperature. The samples were placed in the tube and a thinner tube containing DMSO-D₆ was inserted, allowing to recover the oil-samples without modification after the analysis. In order to quantify the organic functions in the bio-oil, trioxane was diluted in DMSO-D₆ with a concentration of 2.7 % wt. %. The choice of trioxane is due to its specific chemical shift (at 93 ppm) that is well defined and does not overlap with other peaks of the bio-oils.

The organic fraction of bio-oils was analyzed using a gas chromatograph coupled with a mass spectrometer (Shimadzu GCMS-QP2010 SE) equipped with a Zebron ZB Wax-Plus column (Phenomenex) 60 m, 0.25 mm I.D., film thickness 0.25 μm. The oven temperature program starts at 70 °C (hold for 10 min), then heating rate of 5 °C/min up to 150 °C. At this point the heating rate changes to 3 °C/min up to 250 °C (hold for 15 min).

The two-dimensional gas chromatography coupled with mass spectrometry (GCxGC-MS) was carried out in equipment from Agilent (GC 6890 N). The first separation was performed by a polar column VF-1701 MS (I.D 0.25 mm; Film thickness 0.25 μm; length 30 m) followed by a second column apolar DB1 (I.D 0.25 mm; Film thickness 0.25 μm; length 1.5 m) to promote the second dimension of separation. The modulation was performed by a cryogenic modulator from Zoex Corporation (USA) at each 12 s. Compounds were identified by the coupled MS detector (5975B). This inversed configuration (with polar column first) gives a better characterization of oxygen and nitrogen containing compounds as well as hydrocarbons [18].

Regarding the temperature program, the first oven (first column) starts at 50 °C–300 °C with a heating rate of 1.75 °C/min, then, the heating rate changes to 1.8 °C/min and the temperature is increased to 320 °C, while the second oven goes from 50 °C to 320 °C at 1.8 °C/min. The sample were prepared by diluting the oil in methanol at a concentration of 20 wt.%.

3. Results and discussion

3.1. Biomass characterization

The main properties of beech wood chips are summarized in Table 1.

The Higher Heating Value was calculated from the elemental analysis using the equation proposed by Channiwala and Parikh [19] as reported below.

$$\text{HHV} = 0.3491[\text{C}] + 1.1783[\text{H}] - 0.1034[\text{O}] - 0.0151[\text{N}] - 0.0211[\text{ASH}]$$

The calculated HHV is expressed in MJ/Kg and [C], [H], [N], [O] and [ASH] are expressed in mass percentages on dry basis. This equation is valid for the specific range of values, i. e. C: 0.00–92.25 %; H: 0.43–25.15%; O: 0.00–50.00%; N: 0.00–5.60%; Ash: 0.00–71.40%.

Table 1
Properties of beech wood.

Property	Beech wood
Bulk density (ρ_{bulk})	0.31 kg/L
Moisture	7 ± 1 (%wt.)
Elemental analysis (wt. %)	
C	50.3 ± 0.2
H	5.4 ± 0.2
N	0.1 ± 0.04
*O	44.2 ± 0.3
Estimated Higher Heating Value (HHV)	19.3 ± 0.3 MJ/Kg
Ash content	0.9 ± 0.1 (%wt.)
Extractives (%wt.)	
n-hexane	0.16 ± 0.02
acetone	0.69 ± 0.08

* -Obtained by difference.

The total amount of extractible compounds was less than 1 wt.%, with a higher amount extracted in acetone (polar solvent) than in n-hexane (apolar), which agrees with the low lipid contents expected in wood. Regarding the extractives found in beech wood, Zule and Može [16] reported the presence of hydrophobic lipids in hexane extract (≈ 0.1 wt. %) whereas polar compounds, such as low molecular weight sugars and phenolic compounds, were found in acetone extracts (total amount 0.7 wt. %).

TGA analyses were performed under air (Fig. S1) and under N_2 (Fig. S2) to accurately assess the amounts of inorganic ashes and non-volatile (chars) residues, respectively, in the beech wood used in pyrolysis experiments. The amount of inorganic ashes after TGA in air was 1.6 wt.% at 900 °C, this amount being probably more accurate than the one determined by simple calcination of wood (Table 1). Under nitrogen, the solid residue (mixture of char and inorganic compounds) at the pyrolysis reaction temperature (500 °C) was approximately 23 wt.%.

Aiming to obtain more information about the composition of biomass and to identify the presence of inorganic components, such as metals, that may have an influence on the pyrolysis process, the ashes were analyzed using SEM-EDS (semi-quantitative analysis). Table 2 shows the respective concentration of elements found.

Since the SEM images showed that the ash particles were visually heterogeneous, these values were calculated as an average of analyses collected at 11 different spots. It was possible to identify 14 elements, the most abundant being Ca and K. The compositions analyzed at different sample location were also heterogeneous, which translates in the large values of absolute errors, leading, in some cases, to numbers without statistical significance (for instance, as observed for Al and Cl).

3.2. Catalyst characterization

The elemental composition of the prepared catalysts was determined using ICP and the results are presented in Table 3.

The diffractograms for the catalysts studied are displayed in Fig. 2.

The first diffractogram shows the typical MFI structure, characteristic of zeolites H-ZSM-5, with the main lines between 7–9° and 22–25° that correspond to an orthorhombic structure [20–22].

Fig. 4b shows the diffractograms for metal mixed oxides and pure niobium oxide. The structures found are listed in Table 4.

The catalyst prepared with only Nb precursor corresponds to a pure orthorhombic Nb_2O_5 phase. Similarly, the main reflection of the Nb_2O_5 phase (near 23°) is observed for all $Nb_xM_yO_z$ catalysts. The $Nb_xW_yO_z$ catalyst was very poorly crystallized and mostly amorphous, except for the main reflections of Nb_2O_5 . According to the literature [23], the substitution of Nb for W in Wb-Nb-O mixed oxides results in a progressive loss of crystallinity. Given the similarity between the ionic radii in octahedral coordination ($r^{VI}Nb^{5+} = 0.64$ Å, $r^{VI}W^{6+} = 0.60$ Å [24]), a solid solution can be formed by partial substitution of W cations in the Nb_2O_5 lattice.

The $Nb_xAl_yO_z$ catalyst exhibited only the diffraction lines of

Table 3

Chemical composition catalysts and relevant atomic ratios.

Catalyst	Nb (wt. %)	M (wt. %) M = W, Al or Mn	Nb/M atomic ratio	Si/Al atomic ratio
$Nb_xW_yO_z$	25.6	39.1	1.37	–
$Nb_xAl_yO_z$	50.5	11.0	1.33	–
$Nb_xMn_yO_z$	47.4	20.5	1.30	–
H-ZSM-5	–	–	–	40.5

orthorhombic Nb_2O_5 and there was no evidence of Al_2O_3 phases, which is in agreement with literature [25].

The $Nb_xMn_yO_z$ catalyst was well crystallized and exhibited several reflections in addition to those corresponding to Nb_2O_5 : Nb_2MnO_6 , Mn_3O_4 and Mn_2O_3 could be identified in the diffractogram. Lian and co-workers [26] observed similar phases in Nb/Mn mixed oxides, except Mn_3O_4 . However, it is noteworthy that these authors calcined the catalysts at 500 °C. Therefore, the presence of Mn_3O_4 could be related to the higher temperature of calcination (600 °C) that leads to the conversion of Mn_2O_3 into Mn_3O_4 [27]. Besides the formation of a Nb_2MnO_6 mixed phase, however, the presence of several pure Mn phases suggests that the Nb_2O_5 structure can accommodate only a limited amount of Mn cations in its lattice, possibly because Mn^{3+} cations are more stable in a cubic coordination.

The textural properties of catalysts are presented in Table 5.

The specific surface areas (SSA) of the Nb-based catalysts calcined at 600 °C are in the range 26–93 m^2/g , which is the range expected for citrate gel synthesis of metal oxides and treated at similar temperature. The calcination temperature of 600 °C was chosen higher than the pyrolysis temperature to ensure that the catalysts structural and textural properties were fully stabilized and to prevent catalyst sintering during the catalytic tests. Yang and co-workers [15] obtained surface values of 108 m^2/g and 150 m^2/g for $Nb_xW_yO_z$ and $Nb_xAl_yO_z$, respectively, however after calcination at 500 °C. Higher temperatures led to sintering of metal oxides, resulting in a reduction of SSA and porous volume, as demonstrated by Yang et al. [15] in the same work. Lian and collaborators [26] evaluated a catalyst based on Nb and Mn calcined at 500 °C and found specific area of 58 m^2/g , which is higher than observed at this work, but the same justification related to the higher calcination temperature can be employed here. In contrast, the SSA of H-ZSM-5 is much higher, but H-ZSM-5 is a microporous solid and its high SSA corresponds essentially to the surface of the micropores.

The increase in the specific area of $Nb_xW_yO_z$ compared to pure Nb_2O_5 agrees with literature. According to Jehng et al. [28], the particle sintering that leads to the reduction of surface area is related to surface dihydroxylation of amorphous Nb_2O_5 to form crystalline Nb_2O_5 , and the presence of a second metal oxide can partly inhibit the dihydroxylation and therefore sintering. The material can retain the textural properties even when calcined at high temperature (500 °C). In addition, the authors reported that this effect depends on the interaction of the second metal with the niobium oxide, in the way that the higher is this interaction, the higher the resulting surface.

Delgado and co-workers [23] evaluated the influence of Nb concentration on the textural properties of mixed metal oxides with tungsten. The authors reported that for low Nb/W molar ratios the specific area was lowered by a reduction of mesopores. These modifications were ascribed to alterations at crystalline structure due to isomorphous substitution of W by Nb in the lattice, given their similar ionic radius ($r^{VI}Nb^{5+} = 0.64$ Å, $r^{VI}W^{6+} = 0.60$ Å).

The total acidity of catalysts was measured using NH_3 -TPD. The TPD profiles of Nb-based catalysts (Fig. 3) could be decomposed into two main Gaussian peaks centered at 187 ± 3 and 281 ± 8 °C, which represented ≈ 30 % and ≈ 70 % of the total surface, respectively. The maximum temperature of the second peak varied in the order: Nb < Nb-Mn < Nb-Al < Nb-W, suggesting that the acidity strength increased is

Table 2

Composition of ashes derived from beech wood obtained by SEM-EDS.

Component	wt. %
O	39 ± 7
Na	0.5 ± 0.3
Mg	6 ± 2
Al	0.1 ± 0.3
Si	0.5 ± 0.3
P	1.3 ± 0.5
S	2 ± 1
Cl	0.09 ± 0.4
K	19 ± 9
Ca	29 ± 11
Mn	2 ± 1

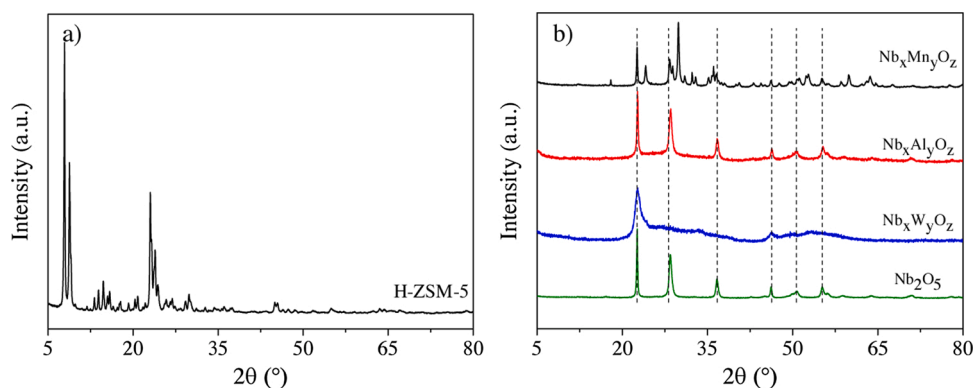


Fig. 2. X-ray diffractograms for a) H-ZSM-5 and b) mixed metal oxides.

Table 4

Crystalline phases identified in catalyst diffractograms.

Catalyst	Formula	System	a (Å)	b (Å)	c (Å)
Nb ₂ O ₅	Nb ₂ O ₅	Orthorhombic	6.2	29.2	3.9
Nb _x W _y O _z	Nb _{6.7} W _{10.3} O ₄₇	Orthorhombic	12.3	36.6	3.9
Nb _x Al _y O _z	Nb ₂ O ₅	Orthorhombic	3.6	–	3.9
	Nb ₂ MnO ₆	Orthorhombic	14.4	5.8	5.1
Nb _x Mn _y O _z	Nb ₂ O ₅	Orthorhombic	6.2	29.2	3.9
	Mn ₃ O ₄	Tetragonal	5.8	–	9.5
	Mn ₂ O ₃	Cubic	9.4	–	–

Table 5

Textural properties of catalysts.

Catalyst	S _{BET} ^a (m ² g ⁻¹)	Average pore diameter ^b (nm)	Total pore volume (cm ³ g ⁻¹)
Nb ₂ O ₅	26	18	0.12
Nb _x W _y O _z	44	9	0.09
Nb _x Al _y O _z	93	8	0.20
Nb _x Mn _y O _z	26	12	0.08
H-ZSM-5	423	0.55 ^c	0.18

^a BET surface.

^b Obtained by BJH method.

^c from International Zeolite Association database.

this order. In comparison, these peaks were shifted at 204 °C (53 %) and 401 °C (47 %) in H-ZSM-5 NH₃-TPD profiles, and the desorption continued at 600 °C. The total amounts of acid sites are reported in Table 6. They agree with the total numbers of acid sites reported by Yang et al. for Nb-based mixed oxides [15]. Although H-ZSM-5 exhibits the highest amount of acid sites on a mass basis, it is interesting to note that the Nb-based mixed oxides present a 2–3 time higher density of acid sites per surface area than the zeolite.

Transmission IR spectroscopy of pyridine adsorbed on the catalysts was used to assess more specifically the type of acid sites present on the surface. The spectra are displayed in Fig. 4.

The adsorption bands at 1545 and 1455 cm⁻¹ can be assigned to Brønsted and Lewis sites, respectively. The band at 1490 cm⁻¹ is attributed to the combination of these two types of acid sites [29]. In addition, the bands at 1615 and 1623 cm⁻¹ are assigned to Lewis acid sites with weak and strong acid strength, respectively [30]. Table 6 shows the quantification of Brønsted and Lewis acid sites expressed as a function of mass of catalyst as well as its specific area.

In agreement with NH₃-TPD, H-ZSM-5 showed the highest concentration of acid sites referred to the mass of catalyst. Furthermore, H-ZSM-5 exhibited a high concentration of Brønsted sites, while the Nb oxides solids present essentially Lewis sites, which is in agreement with the literature [15,31–33]. However, due to the large difference in specific surface areas, the acid sites concentrations are not so different when

referred to the catalyst BET surface areas.

Niobic acid (hydrated niobium oxide) exhibits a high density of Brønsted acid sites when calcined at moderate temperature (< 300 °C), whereas surface dehydroxylation by calcination at 400 °C leads to the formation of coordinatively unsaturated Nb cations that behave as strong Lewis sites [34]. The Brønsted sites have been reported to be fully eliminated after calcination at 580 °C (under dry conditions); consistently, the Nb₂O₅ catalyst prepared in the present study, which has been calcined at 600 °C, exhibits only Lewis sites.

W, Al and Mn oxides are also solid acids. WO₃ presents strong B and L sites, whereas γ-Al₂O₃ presents a weak Brønsted acidity and strong Lewis sites. Similarly, MnO₂ (obtained by calcination at 400 °C) and Mn₂O₃ (obtained by calcination at 600 °C) exhibit Lewis acid sites, which are much stronger for the latter [35]. The B/L ratio of oxide surfaces depends on the calcination temperature and on the presence or absence of steam, since Brønsted acidity also arises from acid-base complexation of Lewis sites by water molecules [36]. Regarding the bimetallic metal oxides, Table 6 shows that the presence of a second metal increased the amount of Lewis and Brønsted acid sites. Datka et al. [37] studied the effect of impregnation of niobium oxides over different metallic oxides supports, such as Al₂O₃ and they reported that the creation of acidity is associated with the formation of bridging hydroxyls between the niobium and aluminum cations. In addition, Yamashita et al. [38] observed that the presence of tungsten oxide created Brønsted acid sites when mixed with niobium oxide.

3.3. Catalytic treatment of pyrolysis vapors

The effect of catalysts on the conversion of beech wood pyrolysis vapors was assessed by comparing purely thermal experiments with runs performed in the presence of catalysts placed in the reactor directly at the outlet of the pyrolysis zone (Fig. 1).

3.3.1. Mass balance and products distribution in pyrolysis experiments

The mass of gas, solid and liquid products and the global mass balance of the pyrolysis experiments with or without catalytic conversion of vapors are presented in Table 7. Triplicate experiments were run without catalyst and with the Nb_xW_yO_z catalyst to assess the reproducibility of the results.

The mass balance was close to 100 % for all samples, except in the experiment with Nb_xAl_yO_z. This may result from a total wood injection above average in this experiment.

The selectivity for each phase is presented in Fig. 5.

The error bars displayed in this graphic were obtained from the triplicate experiments without catalyst and with the Nb_xW_yO_z catalyst.

The solid fraction was similar in all experiments (≈19 wt.%) and in good agreement with that obtained in TGA experiments on beech wood under N₂ (Fig. S2). Since the solid is formed in the reactor before any contact of the reaction products with the catalyst bed, the presence of

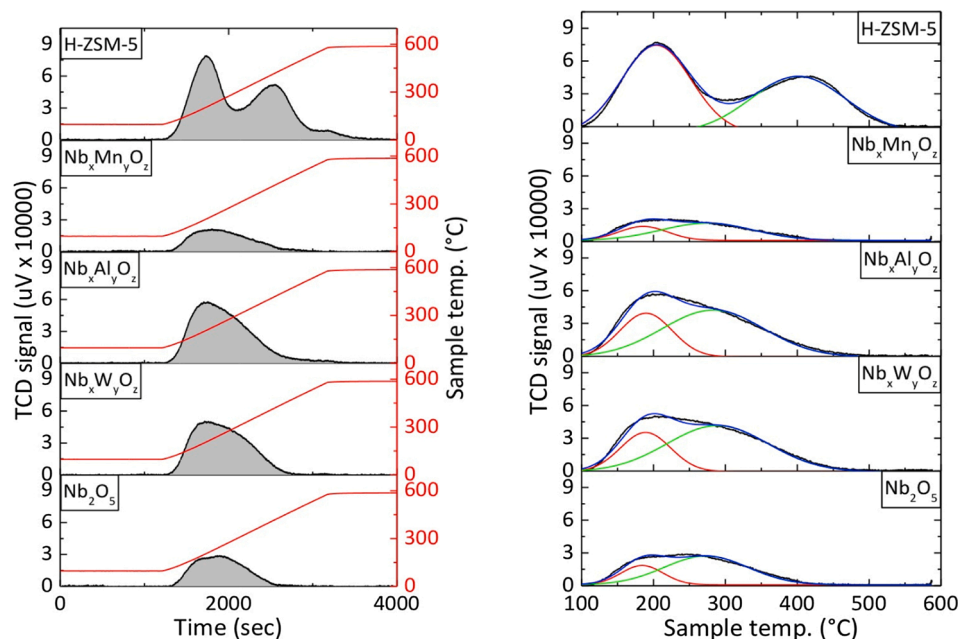


Fig. 3. NH_3 -TPD profiles of Nb-based and H-ZSM-5 catalysts.

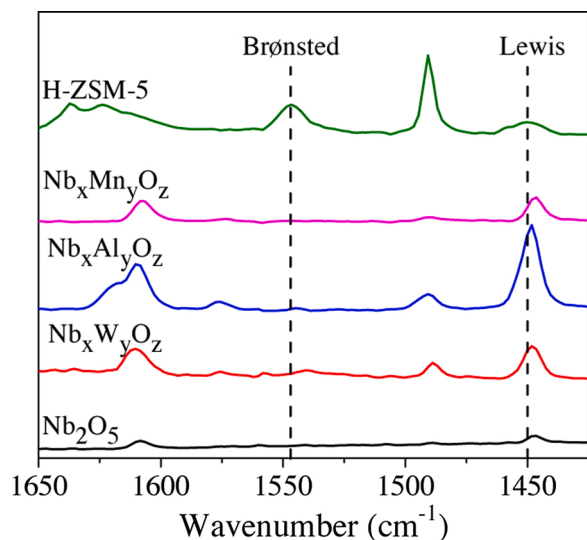


Fig. 4. IR spectra of pyridine adsorbed at 150 °C.

Table 6

Acidic properties of catalysts measured by NH_3 -TPD and IR of pyridine adsorbed at 150 °C.

Catalyst	NH_3 -TPD		IR/ pyridine			
	Total acidity		Brønsted acid sites		Lewis acid sites	
	$\mu\text{mol/g}$	$\mu\text{mol/m}^2$	$\mu\text{mol/g}$	$\mu\text{mol/m}^2$	$\mu\text{mol/g}$	$\mu\text{mol/m}^2$
Nb_2O_5	89.9	3.46	n.d.	n.d.	7	0.27
$\text{Nb}_x\text{W}_y\text{O}_z$	176.3	4.01	9	0.22	26	0.62
$\text{Nb}_x\text{Al}_y\text{O}_z$	201.4	2.17	2	0.02	90	0.97
$\text{Nb}_x\text{Mn}_y\text{O}_z$	75.1	2.89	n.d.	n.d.	19	0.71
H-ZSM-5	501.0	1.18	127	0.30	45	0.11

n.d. : not detected (below detection limits).

catalysts is not expected to affect the formation of the solid fraction. A significant increase in the gas phase selectivity, associated to a decrease in liquid phase selectivity, was observed with the H-ZSM-5 catalyst, and

Table 7

Mass of gas, liquid and solid products and overall mass balance of experiments.

Catalyst	Mass (g)			Total mass (g) / Mass balance
	Gas phase	Liquid phase	Solid phase	
Without catalyst	5.1	12.0	4.0	21.0 / 103 %
3 experiments	3.5	11.3	3.8	18.6 / 91 %
	4.2	10.9	3.9	18.9 / 92 %
Average \pm SD	4.27 \pm 0.80	11.4 \pm 0.56	3.9 \pm 0.10	
Nb_2O_5	4.8	11.4	4.0	20.2 / 99 %
$\text{Nb}_x\text{W}_y\text{O}_z$	5.2	11.7	4.0	20.9 / 102 %
3 experiments	4.9	12.2	4.5	21.6 / 105 %
	4.9	10.5	4.1	19.5 / 95 %
Average \pm SD	5.0 \pm 0.17	11.47 \pm 0.87	4.2 \pm 0.26	
$\text{Nb}_x\text{Al}_y\text{O}_z$	7.7	12.1	4.2	24.0 / 117 %
$\text{Nb}_x\text{Mn}_y\text{O}_z$	7.2	10.8	4.1	22.1 / 108 %
H-ZSM-5	8.4	9.7	3.9	22.0 / 107 %

to a smaller extent with $\text{Nb}_x\text{Al}_y\text{O}_z$ and $\text{Nb}_x\text{Mn}_y\text{O}_z$ catalysts. This behavior can be assigned to the acidic properties of catalysts that favor cracking reactions of vapor stream components, resulting in a formation of light and non-condensable compounds.

3.3.2. Characterization of gaseous products

The total mass flow of the gas phase as a function of time for all experiments is presented in Fig. 6.

The H-ZSM-5 catalyst exhibited the highest production of gaseous products when compared to other catalysts throughout all experiment duration, but the $\text{Nb}_x\text{Al}_y\text{O}_z$ and $\text{Nb}_x\text{Mn}_y\text{O}_z$ catalysts produced almost similar quantities. In contrast, the presence of Nb_2O_5 and $\text{Nb}_x\text{W}_y\text{O}_z$ catalysts did not modify the formation of gas phase products compared to the thermal reaction. The production of gases did not stop immediately when the injection of wood chips was cut off, but it declined rapidly within ≈ 15 min. This indicates that the pyrolysis of wood residues (that are collected on the first frit, before the catalyst bed) continues in the reactor until they are fully converted into char.

In order to understand the impact of catalyst on product distribution

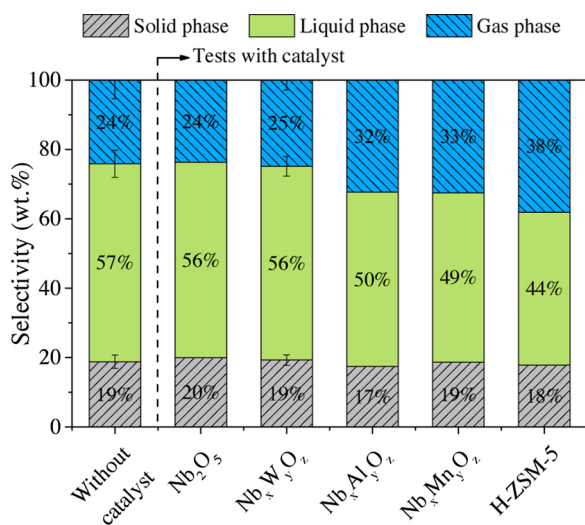


Fig. 5. Selectivity into solid, liquid and gas products.

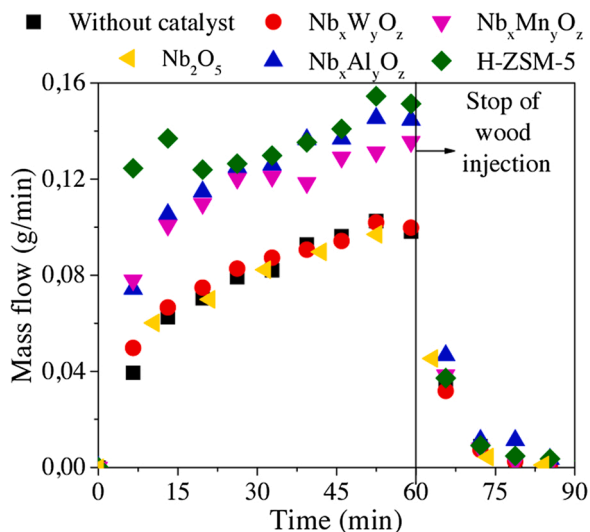


Fig. 6. Total mass flow of gas phase products as a function of time.

on gas phase, the accumulated mass of different products families is presented in Fig. 7.

CO_x compounds accounted for more than 85 % of the total mass of gaseous products, followed by hydrocarbons with 1, 2 and 3 carbons (representing 12 wt.% in average, for the most part methane) and, finally H_2 , (corresponding to less than 1 wt.% of all gas phase products, or ≈ 3.7 mol.%). According to the literature [39], the effect of acidic catalysts, and particularly H-ZSM-5, is to remove oxygen as H_2O and CO_x . As expected from the mass balance data, H-ZSM-5, $Nb_xAl_zO_z$ and $Nb_xMn_yO_z$ catalysts led to an increase in the yields of hydrocarbons, CO_x and H_2 . The increase in light hydrocarbons production corroborates the hypothesis about the occurrence of cracking reactions in the presence of catalysts and more particularly in the case of H-ZSM-5, which has the highest concentration of acid sites.

3.3.3. Characterization of liquid products

Fig. 8 shows the amounts of liquid products formed in pyrolysis experiments. They were mostly collected directly in the first cold trap downstream the reactor. Except for pyrolysis in the absence of catalyst that produced a single liquid phase, all catalysts promoted changes in this liquid fraction composition that resulted in its separation into two immiscible liquids by centrifugation, i.e. a light orange/brown aqueous

phase on top of a dark brown organic phase. When phase separation occurred, this aqueous phase accounted for 26–37 % of the total liquid mass, as shown in Fig. 8.

Another fraction (denoted as “recovered organic phase”) remained stuck on the glassware in the two cold traps and in the electrostatic trap and was recovered by washing them with methanol, followed by evaporation of the solvent. A significant fraction was also found in the subsequent traps (Pyrex and silicagel beads), denoted as “not recovered”, which was weighed but not recovered because washing the Pyrex beads would have involved too much solvent, or because it was not possible to extract it from the silicagel.

The overall mass of liquid products was 10.8–12 g with the Nb-based catalysts, and slightly lower with the H-ZSM-5 reference catalyst (9.8 g), which provided however the highest yield in total organic phases (74 %) and the lowest in aqueous phase.

The bio-oils characterizations reported below were carried out on the organic phase that separated physically from the aqueous phase for the samples obtained in the presence of catalysts (or on the single liquid phase that was obtained without catalyst). The “recovered organic phase” was assumed to have a similar composition but it was only quantified by weighing. Indeed, the recovery process involved washing the glassware with methanol followed by evaporating the solvent, which can modify its composition since the lighter components will evaporate as well. Therefore, the characterizations were made on the raw organic phases which have not undergone any treatment.

The water content of the organic phase was determined by Karl Fischer titration; the values of water content, absolute and relative error are displayed in Table 8.

As expected from the single liquid phase obtained in this case, the sample obtained without catalyst showed the highest water content. Comparing the results obtained using catalysts, the bio-oil produced in presence of H-ZSM-5 has the lowest quantity of water.

The molar mass distributions are presented in Fig. 9. The peak intensities are normalized to the maximum intensity.

As a first observation, the MW range of bio-oil components was relatively low, since the MWs below 260 g/mol accounted for at least 70 % of the chromatograms total surface areas for all samples (this limit corresponds approximately to the maximum MW of compounds that can be analyzed by GC methods). For the thermal bio-oil, the maximum intensity was observed at 168 g/mol, with shoulders at 116, 142, 200, and 268 g/mol. These MW, however, are probably slightly underestimated because the MW measured for two reference compounds, eugenol (164 g/mol) and DHPMPE (274 g/mol), were found smaller than the real ones, the chromatograms exhibiting their maxima at 158 (−4%) and 234 (−15 %) g/mol, respectively. This difference is due to fact that the hydrodynamic volume of the measured compounds is different from that of the hydrocarbon standards used for calibration. Compared to the non-catalyzed bio-oil, the maximum intensity for the catalyst-processed bio-liquids was slightly shifted to 158–162 g/mol, depending on the catalyst, and the chromatograms exhibited similar shoulders at 116 and ≈ 140 g/mol, but the intensity of these low MW peaks was clearly higher (Fig. 10).

The response of a RI detector in GPC has been shown to be strongly compound-dependent, therefore comparing directly the peaks intensity is valid only for strictly similar compounds [40]. However, since the peak shoulders appear at similar MW in the chromatograms of thermal and catalyzed bio-oils and assuming that the low MW products formed are similar but in different amounts, in the presence of catalysts more low MW products were formed. In the 200–300 g/mol range the trends were difficult to assess because, as shown by Hoekstra et al. [40] using various model compounds in the 180–620 g/mol range, the RID response factor can vary up to a factor of 10 depending on the compound considered.

The average molecular weights of the organic fraction obtained by gel permeation chromatography (GPC) are presented in Table 9.

The average molar masses were close in all experiments, and the

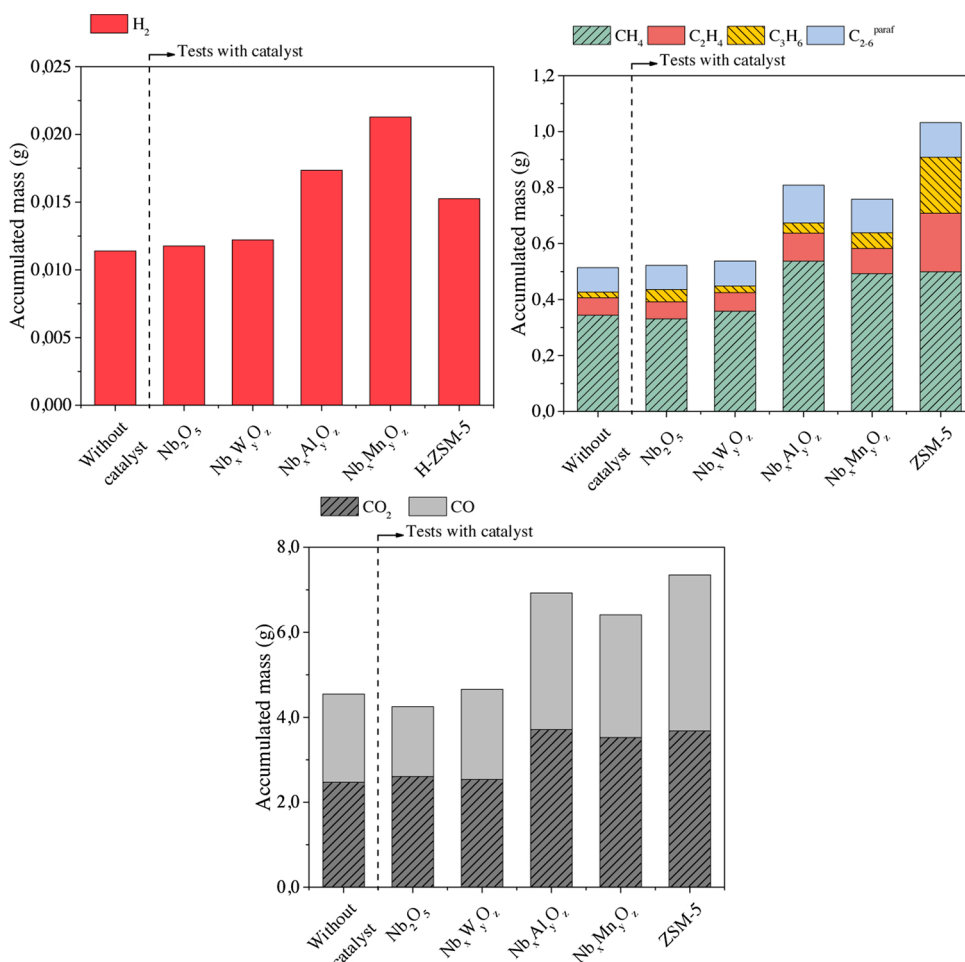


Fig. 7. Accumulated mass of the different gas products in pyrolysis experiments.

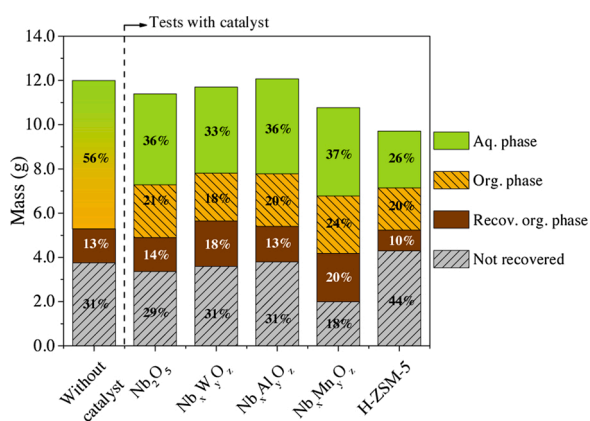


Fig. 8. Mass of organic and aqueous phases recovered in the traps downstream the pyrolysis reactor.

Table 8
Water content and errors for organic phase.

Experiment	Water content	Relative error
Without catalyst	46.3 ± 0.6 %	1.4 %
Nb ₂ O ₅	29.7 ± 1.3 %	4.5 %
Nb _x W _y O _z	27.8 ± 0.3 %	1.2 %
Nb _x Al _y O _z	21.6 ± 0.2 %	0.9 %
Nb _x Mn _y O _z	28.3 ± 0.4 %	1.5 %
ZSM-5	17.9 ± 0.7 %	3.8 %

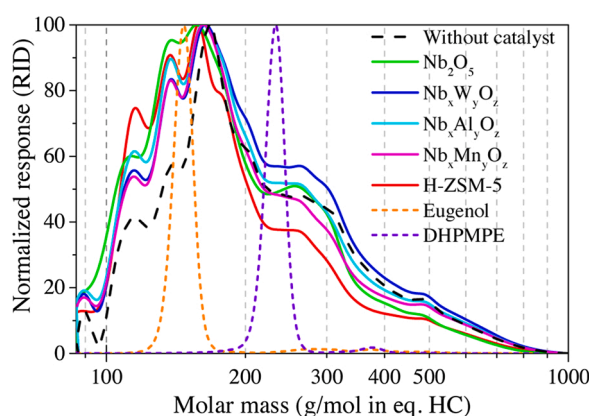


Fig. 9. Molecular mass distribution measured by GPC.

presence of catalysts resulted in a modest but significant decrease in the mean molecular mass. The H-ZSM-5 catalyst resulted in the lowest mean MW. The contact of the pyrolysis products with the acidic catalysts appears to promote the cracking of reaction oligomers, thus decreasing the average molar mass.

GPC analyses using the UV detector operating at 254 nm were also used to obtain a more selective insight on the compounds with aromatic and/or conjugated unsaturated bonds present in the bio-oils. Here, the UV detector signal was here normalized to an equal mass of dry bio-oil injected (100 µg), in order to correct the intensity for small differences in

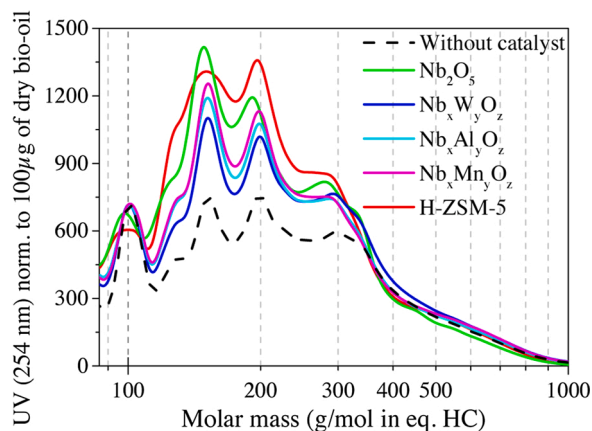


Fig. 10. GPC-UV chromatograms of thermal and catalytically-processed bio-oils, normalized to 100 µg of dry bio-oil.

Table 9

Molecular weight distribution metrics for bio-oils using RI detector (in HC equivalent).

	Number average mass M_n (g/mol)	Weight average mass M_w (g/mol)
Standards		
Eugenol	151	147
DHPMPE	232	234
Bio-oils		
Without catalyst	191	235
Nb_2O_5	172	211
$Nb_xW_yO_z$	185	230
$Nb_xAl_yO_z$	178	221
$Nb_xMn_yO_z$	178	220
H-ZSM-5	167	202

sample dilution and for the different contents of water in each bio-oil (this correction being possible since the absorption of pure water at 254 nm is very weak and can be neglected) (Table 10).

Except for the peak close to 100 g/mol, very intense for the thermal bio-oil, the chromatograms of the catalytically processed bio-oils exhibit higher peaks intensities in the whole 120–350 g/mol range compared to the thermal bio-oil. This suggests that higher amounts of aromatic/conjugated compounds in this MW range are formed in the presence of catalysts, which could result from a better depolymerization of lignin.

The elemental compositions and estimated HHV of bio-oil samples are presented in Fig. 11. It is worth mentioning that sulfur S was also analyzed but found below the detection limit (≈ 0.075 wt%) in all samples. The Higher Heating Value (HHV) was calculated applying the

Table 10

Elemental composition and estimated HHV of the organic phase.

	Elemental composition (dry basis)				HHV (MJ/Kg)
	C (wt%)	H (wt%)	N (wt%)	O* (wt%)	
Without catalyst	63.4 ± 1.5	4.9 ± 0.1	3.0 ± 1.8	28.6 ± 0.2	25.0
Nb_2O_5	70.0 ± 2.0	6.0 ± 0.5	1.0 ± 0.6	23.0 ± 2.2	29.1
$Nb_xW_yO_z$	70.3 ± 0.9	5.5 ± 0.2	1.1 ± 0.8	23.1 ± 1.5	28.6
$Nb_xAl_yO_z$	70.6 ± 0.3	5.8 ± 0.1	1.1 ± 0.2	22.6 ± 0.4	29.1
$Nb_xMn_yO_z$	75.7 ± 1.3	5.2 ± 0.1	1.6 ± 0.5	17.6 ± 1.0	30.7
H-ZSM-5	76.9 ± 0.1	5.5 ± 0.2	2.2 ± 1.4	15.4 ± 1.7	31.8

* -obtained by difference.

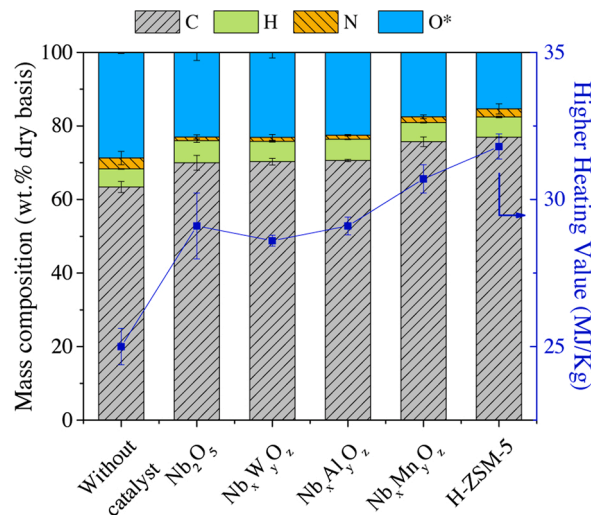


Fig. 11. Elemental composition of bio-oils and calculated HHV (*: oxygen content calculated by difference).

equation proposed by Channiwal and Parikh [19].

The presence of catalysts always resulted in a decrease in the oxygen content compared to non-catalyzed bio-oil, the reference catalyst (H-ZSM-5) showing the highest reduction level (≈ 46 %). Among the Nb-based oxides, the $Nb_xMn_yO_z$ catalyst showed the highest deoxygenating behavior (-39 %). Consequently, the HHV of the catalyst-processed bio-liquids are higher (25 MJ/kg without catalyst and 31.8 MJ/kg with H-ZSM-5) of nearly 27 %. Compared to literature data, the estimated HHV values are slightly higher than usually found for bio-oil produced from woody biomass in the absence of catalysts [41–43,17].

The Van Krevelen representation of the O/C and H/C molar ratios (calculated on dry basis) is presented in Fig. 12.

The effect of catalysts is more pronounced on the O/C ratio than on the H/C ratio. The highest oxygen content reduction is obtained with H-ZSM-5 and $Nb_xMn_yO_z$ catalysts: The O/C ratio of 0.68 in the initial biomass is reduced to 0.15 and 0.17, respectively, vs. 0.34 for the thermal bio-oil.

Despite the importance of oxygen removal for improving bio-oil quality, it should not be the only factor considered to assess the quality of upgraded bio-oils. As discussed by Venderbosch [44], in some cases the presence of oxygenated compounds can be beneficial to the fuel properties, for example methanol and ethanol, which contain respectively 50 and 25 wt% of oxygen. Conversely, the partial

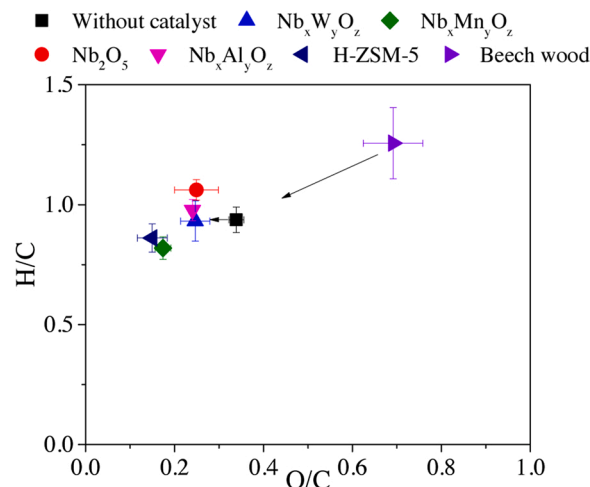


Fig. 12. O/C and H/C molar ratios in the organic phase for different catalysts.

polymerization of compounds may reduce the oxygen content in liquid fuels obtained from pyrolysis of biomass, but also result in an increase of viscosity. Therefore, it is also important to evaluate the chemical modifications promoted by the presence of catalysts.

In this sense, ^{13}C -NMR is a useful technique given its ability to identify the different functional groups containing carbon. The chemical shift range for each functional group are summarized in Table 11.

The ^{13}C -NMR carbon distribution of functional groups in the organic liquids obtained for each experiment is displayed in Fig. 13.

Among the catalysts evaluated, H-ZSM-5 promoted the most significant changes on functional groups distribution. However, some trends can be observed regarding the impact of catalysts. First, the total aromatics concentration increased, whatever the linkage (C–H, C–O or C–C) considered. The increase in these fractions may be related to a more efficient depolymerization of lignin oligomers in the presence of catalysts [48,49].

The Brønsted acid sites of protonic zeolites are generally considered responsible for the formation of aromatic compounds through cracking and dehydration reactions, but zeolites with Lewis acidity are also active for the isomerization and dehydration of sugars and sugar-derived compounds [50]. In addition, anhydrosugars can be formed from the other fractions of biomass (cellulose and hemicellulose). These anhydrosugars can also lead to aromatic compounds through a series of acid-catalyzed reactions such as dehydration, oligomerization, decarbonylation and decarboxylation [51,52]. Polycyclic aromatic compounds can be formed through cracking reactions of lignin during pyrolysis, these oligomers can be also converted into aromatics through cracking reactions over acidic catalytic sites.

Another important trend observed in Fig. 13 is the reduction of sugar, alcohol, ether and carboxylic acids and derivatives. Further than reducing the oxygen content on bio-oil, the reduction of these compounds, especially sugars, is important to improve the stability of the bio-oil [53].

It was not possible to observe significant changes regarding the aliphatic C–C bonds, except with H-ZSM-5. As shown previously with the analyses of the gas phase (Fig. 7), this catalyst produced the highest amounts of C_1 – C_3 hydrocarbons, indicating a higher occurrence of cracking reactions, which can result in a reduction of C–C bounds in the liquid phase.

GC–MS analyses provided a more detailed insight on the composition of the bio-liquids. It was not possible to calibrate the GC response for all detected compounds (around 600 different compounds were identified in the different chromatograms [see Supplementary information], but the peak areas of the common compounds found in all chromatograms can be compared to assess the trends related to the effect of catalysts [54–56]. Furthermore, given the vast amount of compounds, the

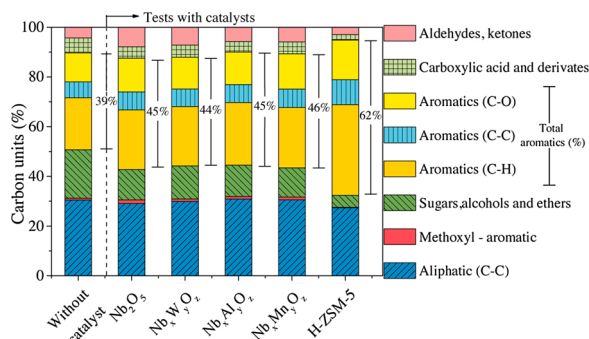


Fig. 13. Organic functions identified with ^{13}C -NMR.

chromatographic resolution may be affected by peak coelution, which makes the compound identification less accurate [57].

Additionally, it is worth mentioning that only compounds that can be volatilized at $250\text{ }^\circ\text{C}$ can be analyzed through this technique, which excludes the heaviest compounds present in bio-oil samples. As an example, the DHPMPE (274 g/mol) used as reference compound in GPC analyses was eluted at the end of the temperature program in GC–MS analyses. However, as shown previously by GPC, at least 70 % of the compounds present in the bio-oils have MW below ≈ 260 g/mol and should be detected in GC methods, provided that they do not decompose in the injector upon heating.

GC–MS analyses enabled the identification of most peaks through their fragmentation pattern, and compounds with similar chemical functions were grouped into compound families. The proposed families and respective examples are presented in Table 12.

These families obtained for all experiments are presented in Fig. 14.

As previously observed with ^{13}C -NMR, the H-ZSM-5 catalyst resulted in the most significant modification on compounds families' selectivity. Besides, some trends are similar for all catalysts. First, the oxygenated aromatic families (aromatic ethers, phenols, guaiacols, syringols) increased. As discussed before, the formation of these compounds is derived from the degradation of lignin (depolymerization), and these reactions of C–C bond cleavage are clearly improved in the presence of all catalysts [58]. The main aromatic compound observed was 2,6-dimethoxy-4-(2-propenyl)-phenol (close to 30 % of the guaiacol/syringol family), which clearly originates from lignin degradation.

Another important modification is the reduction of the sugars, furans and acid/ester family's selectivity. As mentioned before, these compounds contributes to the instability of bio-oils and they are precursors to macromolecules that leads to plugging of reactors and tubing and

Table 11
Chemical shifts for each functional group. Adapted from: [45–47].

Functional group	Range (ppm)	Example
Aldehydes, ketones	180–230	
Carboxylic acid and esters	166–180	
Aromatics	105–166	
–Aromatics (CO)	142–166	
–Aromatics (CC)	132–142	
–Aromatics (CH)	105–132	
Sugars, alcohols and ethers	60.8–105	
Methoxyl - aromatic	55.2–60.8	
Aliphatic (C–C)	0–55.2	

Table 12
Compound families and examples of compounds that represents each group for GC–MS.

Compound family	Examples
Acid/ester	Organic acids (acetic, propanoic, butanoic...), vinyl butyrate
Alcohols	1,2-Ethanediol, Cyclopropyl carbinol
Aldehyde/ketone/ether	1-hydroxy-2-Propanone, cyclopentenones
Aromatics	Benzene, xylene, styrene
Aromatic ether	1,2,4-Trimethoxybenzene, 3,4-Dimethoxytoluene
Furans	2(5H)-Furanone, Furfural, 5-Hydroxymethylfurfural
Guaiacol/syringol	2,6-dimethoxy-phenol, m-Guaiacol, 2,6-dimethoxy-4-(2-propenyl)-phenol
Nitrogen-containing	6-methyl-4(1H)-Pyrimidinone, 3-Methylpyridazine
Other	Dimethyl peroxide, Thiopropionic acid S-isopropyl ester
Polycyclic Aromatic Hydrocarbons (PAH)	Indane, Naphtalenes,
Phenols	Catechols, alkyl-phenols
Sugars	Levoglucosan, D,L-Arabinose, 2,3-Anhydro-D-mannosan

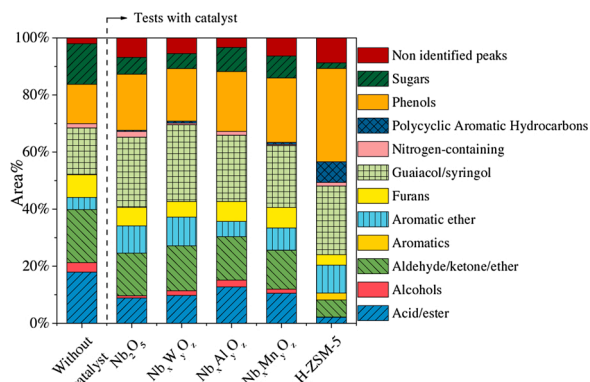


Fig. 14. Compound families analyzed with GC-MS.

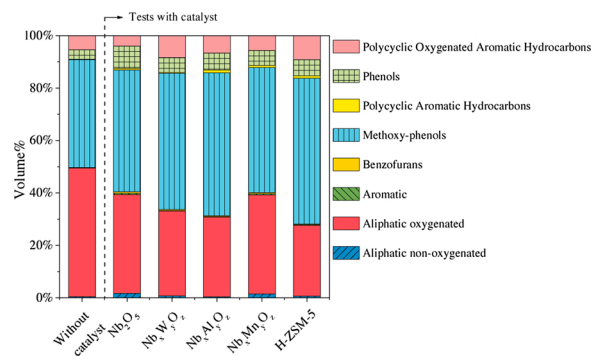


Fig. 15. Compounds families analyzed by GCxGC-MS.

catalyst deactivation by coke deposition [59,60]. The main sugar found in bio-oils was 1,6-anhydro- β -D-glucopyranose (also named as levoglucosan) that can originate from the depolymerization and dehydration of cellulose [61]. Similarly, furans can also be obtained from the dehydration of sugars and depolymerization of hemicellulose [62]. Among the organic acids present in bio-oils, acetic acid was the predominant carboxylic acid present, which is mainly produced from hemicellulose, but it also can be produced from depolymerization of lignin and subsequently release of an acetyl group [48,63]. As reported in the literature, the presence of catalyst can also promote the decarboxylation of carboxylic groups [58].

Due their high polarity, these compounds are probably more soluble in the aqueous phase. Since liquid phase separation was observed for all samples obtained with catalysts, the reduction of these families in the organic phase can also be attributed to their partition during the phase separation. Indeed, GC-GC analyses of the aqueous phase obtained in the presence of HZSM-5 catalyst showed essentially the presence of small organic acids, ketones, aldehydes and some sugars, however in very small amounts compared to the organic phase.

Aiming to improve the resolution of chromatograms, two-dimensional gas chromatography (GCxGC) was used to add a second dimension to the analysis which can result in a better separation of co-eluting compounds. With GCxGC, the volume of the blobs is proportional to the concentration, allowing to compare the trends of compounds families between the different chromatograms, similarly with GC-MS. These groups are represented in Table 13. Due to the different chromatographic conditions between the two techniques (columns nature, maximum allowed temperature, injector temperature) and to the 2D separation of compounds in GCxGC, it was not possible to group the compounds in strictly similar families as with GC-MS (i.e. carboxylic acids/esters had to be grouped with ketones in a common "aliphatic oxygenated" family).

Compounds families' selectivity are represented in Fig. 15.

In agreement with the previous technique, an increase in oxygenated aromatic compounds (phenols and methoxy-phenols) is observed. Additionally, there is a reduction in aliphatic oxygenated compounds. In

Table 13
Compound families and examples of compounds in each group for GCxGC-MS.

Compound family	Examples
Aliphatic non-oxygenated	(E)-2-Hexene, 2,4-dimethyl-2,4-Heptadiene,
Aliphatic oxygenated	Acetic acid, cyclopentenones
Aromatic	Xylenes, styrenes, benzenes.
Benzofurans	Alkyl benzofurans
Methoxy-phenols	2,6-dimethoxy-phenol, m-Guaiacol,
Polycyclic Aromatic Hydrocarbons (PAH)	Naphtalenes, indenes
Phenols	Alkyl phenols, phenol
Polycyclic Oxygenated Aromatic Hydrocarbons (POAH)	Derived from lignin with high molar weight

contrast with GC-MS analyses, it was not possible to identify sugars with GCxGC-MS. This can be related to the injection at higher temperature that can degrade thermosensitive compounds such as sugars [57]. Very few fully deoxygenated aromatic compounds (benzene, toluene, xylenes, styrene, naphthalene...) were detected, even with the H-ZSM-5 catalyst. This contrasts with previously reported studies in which significant yields of such compounds could be produced from either lignin [64] or glucose [65] using H-ZSM-5 catalysts. However, they were obtained at high catalyst/biomass ratios (3/1 or 19/1, respectively) and were related to heavy coke deposition on the zeolite. In the present study the catalyst/biomass ratio was set to 1/10, which appears more realistic from a catalysis standpoint but probably limits the formation of deoxygenated aromatics.

From these two GC-based characterization techniques, common trends such as the reduction in carboxyl and carbonyl groups could be identified. These compounds contribute to deleterious properties of bio-oils, i.e. acidity, instability and corrosiveness [3,66]. The increase in aromatics, resulting from the depolymerization of lignin structure [48, 49,63], is also confirmed by both techniques. And finally, the reduction of sugars and anhydrosugars, these compounds being related to formation of light compounds such as furans and furaldehydes [67] but also sugars-derived polymeric compounds through the caramelization process [68], that can plug tubes or block reactors.

Given the complexity of the processes that can take place during the pyrolysis of biomass and the catalytic upgrading reactions of produced vapors, it was not possible to establish a direct correlation between the acidic properties of catalysts, in terms of Brønsted/Lewis acidity, and the bio-oil properties. H-ZSM-5 showed the most significant changes in bio-oil properties and this catalyst presented the highest concentration of acidic sites per gram of catalyst, particularly Brønsted sites. However, according to IR studies, the very strong Brønsted acid sites of H-ZSM-5 are only present inside the zeolite pores and do not exist on the external surface, whereas Lewis acid sites are present on its external surface area [34]. The $Nb_xMn_yO_z$ catalyst exhibits only Lewis acidity, based on IR of adsorbed pyridine, and a much smaller SSA than H-ZSM-5, but it displays very similar performances on bio-oil upgrading. Surprisingly, both types of acidities appear to lead to similar performances for bio-oil upgrading. A plausible explanation could be that the large amounts of steam present in the pyrolysis vapors generate Brønsted acid sites on the Nb -based catalyst surface under pyrolysis conditions (470 °C). Indeed, the strong effect of steam on the acidity of a Nb_2O_5 catalyst has been evidenced by Omata and Nambu [69]: the activity of niobium oxide for cumene cracking was strongly promoted in the presence of steam, the number of Lewis acid sites decreased and the Brønsted acidity increased in the presence of steam, this effect being reversible. In contrast, a H-ZSM-5 catalyst showed constant activity in presence or absence of steam; the Lewis acidity of H-ZSM-5 also decreased in the presence of steam but its Brønsted acidity did not increase, suggesting that some Lewis sites were poisoned by water. The acidity of ZSM-5 based catalysts has also been shown to be strongly reduced with time on stream during

pyrolysis of oak wood [12]. Clearly, the concentration of acid sites measured on fresh catalysts under dry conditions (Table 6) does not reflect the catalysts acidity under pyrolysis conditions.

The pore size of catalysts should also be taken into consideration: the micropores of H-ZSM-5 (diameter ≈ 0.55 nm) forbid the diffusion of many components of pyrolysis vapors inside the zeolite channels. As an example, the kinetic diameters of compounds such as tetrahydrofuran (0.63 nm), xylitol (0.66 nm) or glucose (0.86 nm, [69]) are already too large for them to diffuse inside the pores of H-ZSM-5, which restricts its active surface to the external surface area for most components of pyrolysis vapors (of the 423 m²/g SSA of H-ZSM-5, 363 correspond to the microporous surface and 60 m²/g to the external surface area). In contrast, the mesopores of Nb-based mixed metal oxides could allow the diffusion of larger compounds and contribute to a better utilization of the available surface acid sites. Finally, increasing the surface areas of Nb-based catalysts could allow improving their activity for the catalytic upgrading of pyrolysis vapors.

4. Conclusions

The catalytic treatment of beech wood pyrolysis vapors was investigated using Nb₂O₅ and Nb_xM_yO_z (M = W, Al, Mn) catalysts, and their performances were compared to a reference H-ZSM-5 catalyst, and to a purely thermal pyrolysis. IR of adsorbed pyridine showed that the catalysts exhibited different acidic properties in terms of number, strength and Brønsted/Lewis ratio. All catalysts modified the yields and composition of the bio-oils produced, to a different extent. The oils obtained with catalysts had an overall lower oxygen content than the thermal oil. GC-MS, GCxGC and ¹³C NMR analyses of the organic phase showed that it contained less aldehydes, ketones, ethers and more aromatics and methoxy phenols compounds. The best Nb-based catalyst, Nb_xM_yO_z, exhibited similar performances for bio-oils upgrading as HZSM-5, in spite of their very different acidic properties. The results suggest that the Lewis acid sites of Nb_xM_yO_z are converted into Brønsted acid in the presence of water vapor produced by pyrolysis of wood, whereas the strongest Brønsted sites of H-ZSM-5 are probably not accessible to most components of the pyrolysis vapors, therefore limiting their role in the upgrading process.

Authors statements

- De Rezende Locatel: investigation, visualization, writing - original draft preparation
- Laurenti: supervision, editing
- Schuurman: editing, funding acquisition
- Guillaume: supervision, visualization, writing - Reviewing & editing.

Declaration of Competing Interest

The authors do not have any conflict of interests to declare.

Acknowledgements

“WASTE2ROAD” project has received funding from the European Union’s Horizon 2020 research and innovation programme under grant agreement N°818120. The authors thank Chantal Lorentz and Ruben-Checa for their valued help with the NMR, GCxGC, CHONS and GPC analyses.

Appendix A. Supplementary data

Supplementary material related to this article can be found, in the online version, at doi:<https://doi.org/10.1016/j.jaap.2021.105241>.

References

- [1] C. of the E.U. European Parliament, 2018, 128.
- [2] R.T.J. Gerards, A. Fernandes, I. Graça, M.F. Ribeiro, Fuel 260 (2020), 116372.
- [3] Md.M. Rahman, R. Liu, J. Cai, Fuel Process. Technol. 180 (2018) 32–46.
- [4] M. Attia, S. Farag, J. Chaouki, Catalysts 10 (2020) 1381.
- [5] F. de Miguel Mercader, M.J. Groeneveld, S.R.A. Kersten, C. Geantet, G. Toussaint, N.W.J. Way, C.J. Schaverien, K.J.A. Hogendoorn, Energy Environ. Sci. 4 (2011) 985.
- [6] M.B. Griffin, K. Iisa, H. Wang, A. Dutta, K.A. Orton, R.J. French, D.M. Santosa, N. Wilson, E. Christensen, C. Nash, K.M. Van Allsburg, F.G. Baddour, D.A. Ruddy, E.C.D. Tan, H. Cai, C. Mukarakate, J.A. Schaidle, Energy Environ. Sci. 11 (2018) 2904–2918.
- [7] D.S. Scott, J. Piskorz, Can. J. Chem. Eng. 62 (1984) 404–412.
- [8] A.V. Bridgwater, Biomass Bioenergy 38 (2012) 68–94.
- [9] G. Yildiz, F. Ronsse, R. van Duren, W. Prins, Renewable Sustainable Energy Rev. 57 (2016) 1596–1610.
- [10] H. Shafaghath, H.W. Lee, Y.F. Tsang, D. Oh, J. Jae, S.-C. Jung, C.H. Ko, S.S. Lam, Y.-K. Park, Chem. Eng. J. 366 (2019) 330–338.
- [11] P.R. Bhoi, A.S. Ouedraogo, V. Soloriu, R. Quirino, Renewable Sustainable Energy Rev. 121 (2020), 109676.
- [12] A.M. Hernández-Giménez, E. Heracleous, E. Pachatouridou, A. Horvat, H. Hernando, D.P. Serrano, A.A. Lappas, P.C.A. Bruijninx, B.M. Weckhuysen, ChemCatChem 13 (2021) 1207–1219.
- [13] B. Luna-Murillo, M. Pala, A.L. Paioni, M. Baldus, F. Ronsse, W. Prins, P.C. A. Bruijninx, B.M. Weckhuysen, ACS Sustainable Chem. Eng. 9 (2021) 291–304.
- [14] L. Dai, N. Zhou, H. Li, W. Deng, Y. Cheng, Y. Wang, Y. Liu, K. Cobb, H. Lei, P. Chen, R. Ruan, J. Anal. Appl. Pyrolysis 149 (2020), 104845.
- [15] P. Yang, S. Fan, Z. Chen, G. Bao, S. Zuo, C. Qi, Appl. Catal. B 239 (2018) 114–124.
- [16] J. Zule, A. Može, J. Sep. Science 26 (2003) 1292–1294.
- [17] A. Margeriat, A. Bouzegane, C. Lorentz, D. Laurenti, N. Guilhaume, C. Mirodatos, C. Geantet, Y. Schuurman, J. Anal. Appl. Pyrolysis 130 (2018) 149–158.
- [18] B. Omais, M. Courtiade, N. Charon, D. Thiébaud, A. Quignard, M.-C. Hennion, J. Chromatogr. A 1218 (2011) 3233–3240.
- [19] S.A. Channiwal, P.P. Parikh, Fuel 81 (2002) 1051–1063.
- [20] Z. Zahara, Y.K. Krisnandi, W. Wibowo, D.A. Nurani, D.U.C. Rahayu, H. Haerudin, AIP Conf. Proc. 2023 (2018), 020088.
- [21] T. Zhao, F. Li, H. Yu, S. Ding, Z. Li, X. Huang, X. Li, X. Wei, Z. Wang, H. Lin, Appl. Catal. A Gen. 575 (2019) 101–110.
- [22] Q. Sheng, K. Ling, Z. Li, L. Zhao, Fuel Process. Technol. 110 (2013) 73–78.
- [23] D. Delgado, A. Fernández-Arroyo, M.E. Domine, E. García-González, J.M. López Nieto, Catal. Sci. Technol. 9 (2019) 3126–3136.
- [24] R.D. Shannon, Acta Cryst A 32 (1976) 751–767.
- [25] S. Carstens, D. Enke, J. Eur. Ceram. Soc. 39 (2019) 2493–2502.
- [26] Z. Lian, F. Liu, H. He, X. Shi, J. Mo, Z. Wu, Chem. Eng. J. 250 (2014) 390–398.
- [27] T. Ohzuku, I. Tari, T. Hirai, Electrochim. Acta 27 (1982) 1049–1053.
- [28] J.-M. Jehng, A.M. Turek, I.E. Wachs, Appl. Catal. A.: General 83 (1992) 179–200.
- [29] Y. Ji, H. Yang, W. Yan, Mol. Catal. 448 (2018) 91–99.
- [30] A. Ungureanu, B. Dragoi, V. Hulea, T. Cacciaguerra, D. Meloni, V. Solinas, E. Dumitriu, Microporous Mesoporous Mater. 163 (2012) 51–64.
- [31] J. Soggi, A. Osatiashiani, G. Kyriakou, T. Bridgwater, Appl. Catal. A Gen. 570 (2019) 218–227.
- [32] R.Liu Nishu, Md.M. Rahman, M. Sarker, M. Chai, C. Li, J. Cai, Fuel Process. Technol. 199 (2020), 106301.
- [33] J. Guo, S. Zhu, Y. Cen, Z. Qin, J. Wang, W. Fan, Appl. Catal. B 200 (2017) 611–619.
- [34] G. Busca, Chem. Rev. 107 (2007) 5366–5410.
- [35] X. Tang, J. Li, L. Sun, J. Hao, Appl. Catal. B 99 (2010) 156–162.
- [36] G. Busca, Catal. Today 41 (1998) 191–206.
- [37] J. Datka, J. Catal. 135 (1992) 186–199.
- [38] K. Yamashita, M. Hirano, K. Okumura, M. Niwa, Catal. Today 118 (2006) 385–391.
- [39] C. Liu, Chem. Soc. Rev. (2014) 31.
- [40] E. Hoekstra, S.R.A. Kersten, A. Tudos, D. Meier, K.J.A. Hogendoorn, J. Anal. Appl. Pyrolysis 91 (2011) 76–88.
- [41] G. Haarlemmer, C. Guizani, S. Anouti, M. Déniel, A. Roubaud, S. Valin, Fuel 174 (2016) 180–188.
- [42] Q. Zhang, J. Chang, T. Wang, Y. Xu, Energy Convers. Manage. 48 (2007) 87–92.
- [43] M. Gholizadeh, X. Hu, Q. Liu, Renewable Sustainable Energy Rev. 114 (2019), 109313.
- [44] R.H. Venderbosch, ChemSusChem 8 (2015) 1306–1316.
- [45] N. Hao, H. Ben, C.G. Yoo, S. Adhikari, A.J. Ragauskas, Energy Fuels 30 (2016) 6863–6880.
- [46] R.M. Happs, K. Iisa, J.R.F. Iii, RSC Adv. 6 (2016) 102665–102670.
- [47] H. Ben, A.J. Ragauskas, Energy Fuels 25 (2011) 2322–2332.
- [48] M. Carrier, M. Windt, B. Ziegler, J. Appelt, B. Saake, D. Meier, A. Bridgwater, ChemSusChem 10 (2017) 3212–3224.
- [49] C.A. Mullen, A.A. Boateng, Fuel Process. Technol. 91 (2010) 1446–1458.
- [50] T. Ennaert, J.V. Aelst, J. Dijkmans, R.D. Clercq, W. Schutyser, M. Dusseleir, D. Verboeckend, B.F. Sels, Chem. Soc. Rev. 45 (2016) 584–611.
- [51] A. Palizdar, S.M. Sadrameli, Fuel 264 (2020), 116813.
- [52] Y.-T. Cheng, G.W. Huber, Green Chem. 14 (2012) 3114.
- [53] J.P. Diebold, A Review of the Chemical and Physical Mechanisms of the Storage Stability of Fast Pyrolysis Bio-Oils, 1999.
- [54] Q. Lu, Z. Zhang, X. Yang, C. Dong, X. Zhu, J. Anal. Appl. Pyrolysis 104 (2013) 139–145.
- [55] X. Lin, L. Kong, H. Cai, Q. Zhang, D. Bi, W. Yi, Fuel Process. Technol. 191 (2019) 71–78.

- [56] A. Pattiya, J.O. Titiloye, A.V. Bridgwater, *J. Anal. Appl. Pyrolysis* (2008) 8.
- [57] M. Staš, M. Auersvald, L. Kejla, D. Vrtiška, J. Kroufek, D. Kubička, *Trac Trends Anal. Chem.* 126 (2020), 115857.
- [58] H. Ben, A.J. Ragauskas, *ACS Sustainable Chem. Eng.* 1 (2013) 316–324.
- [59] M. Ozagac, C. Bertino-Ghera, D. Uzio, A. Quignard, D. Laurenti, C. Geantet, *Biomass Bioenergy* 108 (2018) 501–510.
- [60] S.K.R. Patil, J. Heltzel, C.R.F. Lund, *Energy Fuels* 26 (2012) 5281–5293.
- [61] Q. Lu, X. Ye, Z. Zhang, C. Dong, Y. Zhang, *Bioresour. Technol.* 171 (2014) 10–15.
- [62] T.R. Carlson, J. Jae, Y.-C. Lin, G.A. Tompsett, G.W. Huber, *J. Catal.* 270 (2010) 110–124.
- [63] S. Chu, A.V. Subrahmanyam, G.W. Huber, *Green Chem.* 15 (2013) 125–136.
- [64] C.A. Mullen, A.A. Boateng, *Fuel Process. Technol.* 91 (2010) 1446–1458.
- [65] J. Jae, G.A. Tompsett, A.J. Foster, K.D. Hammond, S.M. Auerbach, R.F. Lobo, G. W. Huber, *J. Catal.* 279 (2011) 257–268.
- [66] A. Imran, E.A. Bramer, K. Seshan, G. Brem, *Fuel Process. Technol.* 127 (2014) 72–79.
- [67] Y.H. Hui (Ed.), *Food Biochemistry and Food Processing*, 1st ed, Blackwell Pub. Professional, Ames, Iowa, 2006.
- [68] D.L. Dalluge, T. Daugaard, P. Johnston, N. Kuzhiyil, M.M. Wright, R.C. Brown, *Green Chem.* 16 (2014) 4144–4155.
- [69] K. Omata, T. Nambu, *Appl. Catal. A Gen.* 607 (2020), 117812.